Minireview

Succinate:quinone oxidoreductases – what can we learn from *Wolinella succinogenes* quinol:fumarate reductase?

C. Roy D. Lancaster*

Max-Planck-Institut für Biophysik, Abteilung Molekulare Membranbiologie, Heinrich-Hoffmann-Str. 7, D-60528 Frankfurt am Main, Germany

Abstract The structure of *Wolinella succinogenes* quinol:fumarate reductase by X-ray crystallography has been determined at 2.2-Å resolution [Lancaster et al. (1999), Nature 402, 377–385]. Based on the structure of the three protein subunits A, B, and C and the arrangement of the six prosthetic groups (a covalently bound FAD, three iron–sulphur clusters, and two haem *b* groups) a pathway of electron transfer from the quinol-oxidising dihaem cytochrome *b* in the membrane to the site of fumarate reduction in the hydrophilic subunit A has been proposed. By combining the results from site-directed mutagenesis, functional and electrochemical characterisation, and X-ray crystallography, a residue was identified which is essential for menaquinol oxidation. [Lancaster et al. (2000), Proc. Natl. Acad. Sci. USA 97, 13051–13056]. The location of this residue in the structure suggests that the coupling of the oxidation of menaquinol to the reduction of fumarate in dihaem-containing succinate:quinone oxidoreductases could be associated with the generation of a transmembrane electrochemical potential. Based on crystallographic analysis of three different crystal forms of the enzyme and the results from site-directed mutagenesis, we have derived a mechanism of fumarate reduction and succinate oxidation [Lancaster et al. (2001) Eur. J. Biochem. 268, 1820–1827], which should be generally relevant throughout the superfamily of succinate:quinone oxidoreductases. © 2001 Federation of European Biochemical Societies. Published by Elsevier Science B.V. All rights reserved.

Key words: Atomic model; Bioenergetics; Fumarate reductase; Membrane protein; Succinate dehydrogenase; X-ray crystallography

1. Introduction

Succinate:quinone oxidoreductases (EC 1.3.5.1) are enzymes that couple the two-electron oxidation of succinate to fumarate (reaction 1) to the two-electron reduction of quinone to quinol (reaction 2):

$$\text{succinate} \rightarrow \text{fumarate} + 2\,H^+ + 2\,e^- \qquad (1)$$

$$\text{quinone} + 2\,H^+ + 2\,e^- \rightarrow \text{quinol} \qquad (2)$$

*Corresponding author. Fax: (49)-69-96 769 423; http://www.mpibp-frankfurt.mpg.de/lancaster/complexII/index.html.
E-mail address: roy.lancaster@mpibp-frankfurt.mpg.de (C.R.D. Lancaster).
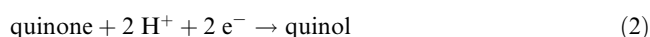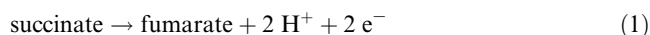
They can also catalyse the opposite reaction, the coupling of quinol oxidation to quinone to the reduction of fumarate to succinate [1]. The *cis*-configuration isomer of fumarate, maleinate, is neither produced in the oxidation reaction, nor is it consumed as a substrate in the reduction reaction, i.e. the reaction is stereospecific in both directions. Depending on the direction of the reaction catalysed in vivo, the members of the superfamily of succinate:quinone oxidoreductases can be classified as either succinate:quinone reductases (SQR) or quinol:fumarate reductases (QFR) [2]. SQR and QFR can be degraded to form succinate dehydrogenase and fumarate reductase (both EC 1.3.99.1), which no longer react with quinone and quinol, respectively.

SQR and QFR complexes are anchored in the cytoplasmic membranes of archaebacteria, eubacteria and in the inner mitochondrial membrane of eukaryotes with the hydrophilic domain extending into the cytoplasm and the mitochondrial matrix, respectively.

SQR (respiratory complex II) is involved in aerobic metabolism as part of the citric acid cycle and of the aerobic respiratory chain [3]. QFR participates in anaerobic respiration with fumarate as the terminal electron acceptor [4,5], and is part of the electron transport chain catalysing the oxidation of various donor substrates (e.g. H_2 or formate) by fumarate. These reactions are coupled via an electrochemical proton potential to ADP phosphorylation with inorganic phosphate by ATP synthase.

Succinate:quinone oxidoreductases generally contain four protein subunits, referred to as A, B, C, and D. Subunits A and B are hydrophilic, whereas the subunits C and D are integral membrane proteins. Among species, subunits A and B have high sequence homology, while that for the hydrophobic subunits is much lower. Most of the SQR enzymes of Gram-positive bacteria and the QFR enzymes from ε-proteobacteria contain only one larger hydrophobic polypeptide (C), which is thought to have evolved from a fusion of the genes for the two smaller subunits C and D [6–8]. While subunit A harbours the site of fumarate reduction and succinate oxidation, the hydrophobic subunit(s) contain the site of quinol oxidation and quinone reduction.

Based on their hydrophobic domain and haem content, succinate:quinone oxidoreductases can be classified in five types (cf. Fig. 1a), according to Hägerhäll and Hederstedt [6] and recently updated by Hederstedt [7]. Type A enzymes contain two hydrophobic subunits and two haem groups, e.g. SQR from the archaea *Archaeoglobus fulgidus*, *Natronomonas*

Fig. 1. *W. succinogenes* QFR, a B-type succinate:quinone oxidoreductase. a: Classification (A–E) of succinate:quinone oxidoreductases based on their hydrophobic domain and haem content [6,7]. The hydrophilic subunits A and B are drawn schematically in blue and red, respectively, the hydrophobic subunits C and D in green or brown. Haem groups are symbolised by yellow rectangles. The directions of the reactions catalysed by SQR and QFR are indicated by red and blue arrows, respectively. White rectangles symbolise the respective cytoplasmic or inner mitochondrial membrane bilayer. The positive (+) and negative (−) sides of the membrane are indicated. In bacteria, the negative side is the cytoplasm, the positive side the periplasm. For mitochondrial systems, these are the mitochondrial matrix and the intermembrane space, respectively. The type of quinone transformed in vivo is not necessarily unique for each type of enzyme. The examples given are thermoplasma quinone (TK), menaquinone (MK), ubiquinone (Q), and caldariella quinone (CQ) [6,39]. See text for further details. b: Three-dimensional structure of the *W. succinogenes* QFR dimer of heterotrimeric complexes of A, B, and C subunits. The Cα traces of the two A subunits are shown in blue and blue-green, those of the two B subunits in red and purple and those of the two C subunits in green and light blue. The atomic structures of the six prosthetic groups per heterotrimer are superimposed for better visibility. From top to bottom, these are the covalently bound FAD, the [2Fe–2S], the [4Fe–4S], and the [3Fe–4S] iron–sulphur centres, the proximal and the distal haem *b* groups. Atomic colour coding is as follows: C, N, O, P, S, and Fe are displayed in yellow, blue, red, light green, green, and orange, respectively. The figure is drawn from the PDB coordinate set 1QLA [8]. The position of bound fumarate close to the isoalloxazine ring of FAD is taken from the coordinate set 1QLB [8]. Figures with atomic models were prepared with a version of Molscript [40] modified for colour ramping [41] and rendered with the program Raster3D [42].

→

pharaonis, and *Thermoplasma acidophilum*. Type B enzymes contain one hydrophobic subunit and two haem groups, as is the case for SQR from the Gram-positive bacteria *Bacillus subtilis*, *Paenibacillus macerans* and QFR from the ε-proteobacteria *Campylobacter jejuni*, *Helicobacter pylori*, and *Wolinella succinogenes*. Examples for type C enzymes, which possess two hydrophobic subunits and one haem group, are SQR from mammalian mitochondria and from the proteobacteria *Paracoccus denitrificans* and *Escherichia coli* and QFR from the nematode *Ascaris suum*. The QFR of *E. coli* is an example for a type D enzyme, which contains two hydrophobic subunits and no haem group. Finally, type E enzymes, such as SQRs from the archaea *Acidianus ambivalens* and *Sulfolobus acidocaldarius*, but also from the proteobacterium *C. jejuni* and the cyanobacterium *Synechocystis* also contain no haem, but have two hydrophobic subunits very different from the other four types and more similar to those of heterodisulphide reductase from methanogenic archaea [9].

Generally, succinate:quinone oxidoreductases contain three iron–sulphur centres, which are exclusively bound by the B subunit. Enzyme types A–D contain one $[2Fe–2S]^{2+,1+}$, one $[4Fe–4S]^{2+,1+}$, and one $[3Fe–4S]^{1+,0}$ centre, whereas an additional [4Fe–4S] centre apparently replaces the [3Fe–4S] in the type E enzyme [10]. The A subunit of all described membrane-bound succinate:quinone oxidoreductase complexes contains a covalently bound FAD prosthetic group [11]. The chemical structure of the linkage as 8α-[Nε-histidyl]FAD was first established for mammalian SQR [12] and subsequently for the QFR enzymes of *W. succinogenes* [13] and *E. coli* [14].

## 2. Overall description of the structure

The currently available crystal structures of succinate:quinone oxidoreductases are those of two prokaryotic QFRs, both since 1999. The *E. coli* QFR, determined at 3.3 Å [15], belongs to the type D enzymes, and the QFR of *W. succinogenes*, refined at 2.2-Å resolution [8] is of type B. Three structures of the latter enzyme, based on three different crystal forms, are available. The first two, PDB entries 1QLA and 1QLB [8], are considerably better defined and more accurate than the structure of the third crystal form, PDB entry 1E7P [16,17], and that of the *E. coli* enzyme, PDB entry 1FUM [15] (see [18] for a discussion). Therefore, the first two crystal forms of *W. succinogenes* QFR will be used for the description of structural features, and those of the third crystal form and of *E. coli* QFR will be referred to for comparison.

In all three *W. succinogenes* QFR crystal forms, two heterotrimeric complexes of A, B, and C subunits are associated in an identical fashion, thus forming a dimer (Fig. 1b). *W. succinogenes* QFR has an overall length of 120 Å in the direction perpendicular to the membrane. Parallel to the membrane, the maximum width is 130 Å for the dimer, and 70 Å for the monomer. Approximately 3665 $Å^2$ (8%) of the *W. succinogenes* QFR monomer surface is buried upon dimer formation. As derived from analytical gel filtration experiments, this dimer is apparently also present in the detergent-solubilised state of the enzyme [18], implying that it is unlikely to be an artifact of crystallisation.

3. Subunit A, the flavoprotein

W. succinogenes QFR subunit A, of 73 kDa [19], is composed of four domains (Fig. 2a), the bipartite FAD-binding domain (blue, residues A1–260 and A366–436, with 'A' indicating the A subunit), into which the capping domain (green, A260–366) is inserted, the helical domain (red, A436–554), and the C-terminal domain (A554–656, not shown in Fig. 2a). The FAD is covalently bound as 8α-[Nε-histidyl]FAD [13] to the residue His A43. The capping domain contributes to burying the otherwise solvent-exposed FAD isoalloxazine ring from the protein surface.

A *W. succinogenes* QFR crystal grown in the presence of fumarate was found to be of crystal form 'B'. The structure was refined at 2.33-Å resolution (PDB entry 1QLB [8]). This allowed the localisation of the fumarate-binding site between the FAD-binding domain and the capping domain next to the plane of the FAD isoalloxazine ring (Fig. 2b). The structure of the enzyme in the third crystal form, 'C' [16] was refined at 3.1-Å resolution (PDB entry 1E7P [17]). Compared with the previous crystal forms, the altered crystal packing [20] results in the capping domain being in a different arrangement relative to the FAD-binding domain (Fig. 2a). This leads to interdomain closure at the fumarate-reducing site, suggesting that the structure encountered in this crystal form represents a closer approximation to the catalytically competent state of the enzyme (Fig. 2b). The *trans* hydrogenation of fumarate to succinate could occur by the combination of the transfer of a hydride ion and of a proton from opposite sides of the fumarate molecule. One of the fumarate methenyl carbon atoms could be reduced by direct hydride transfer from the N5 position of the reduced FADH⁻, while the other fumarate methenyl carbon is protonated by the side chain of Arg A301
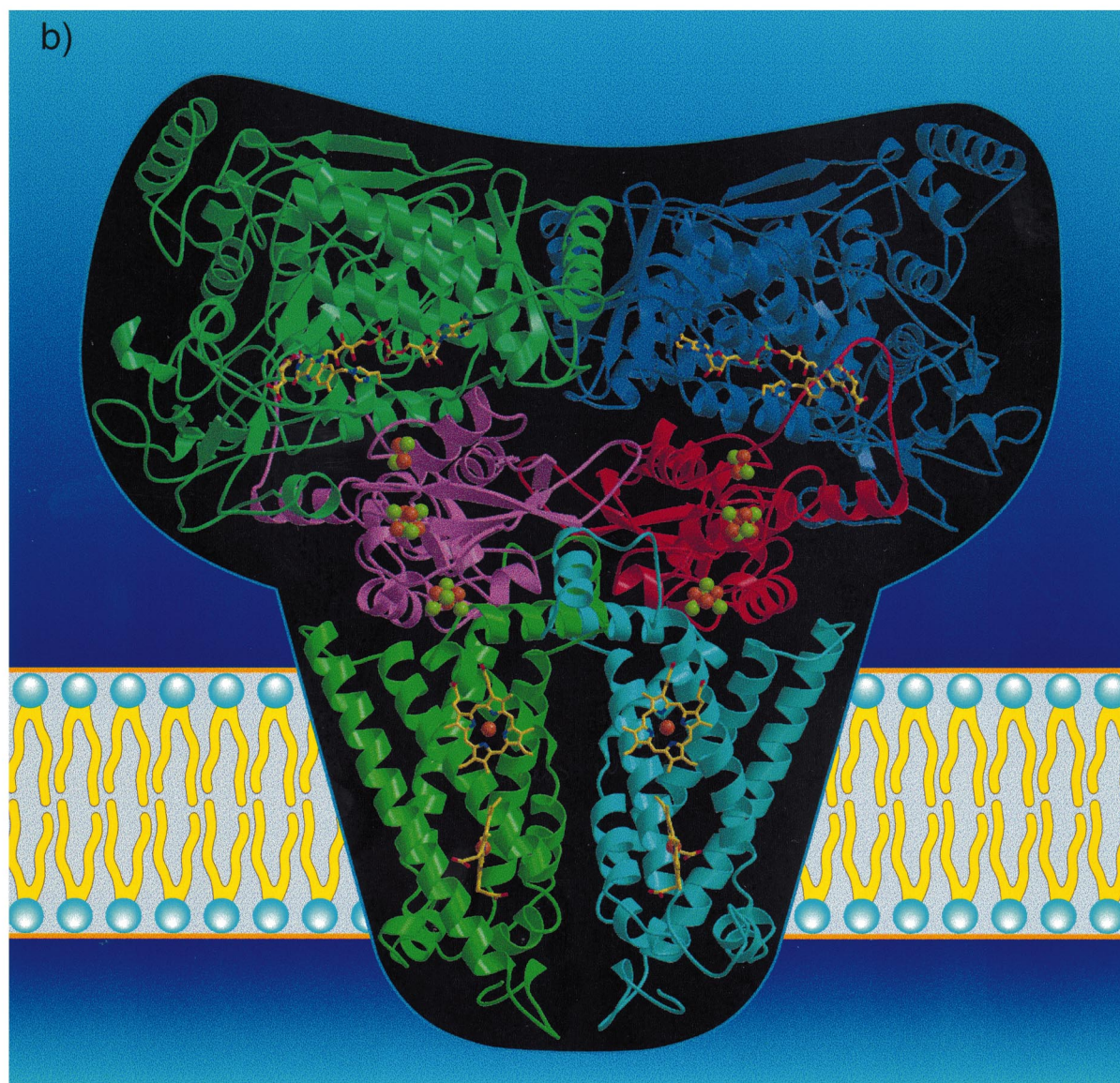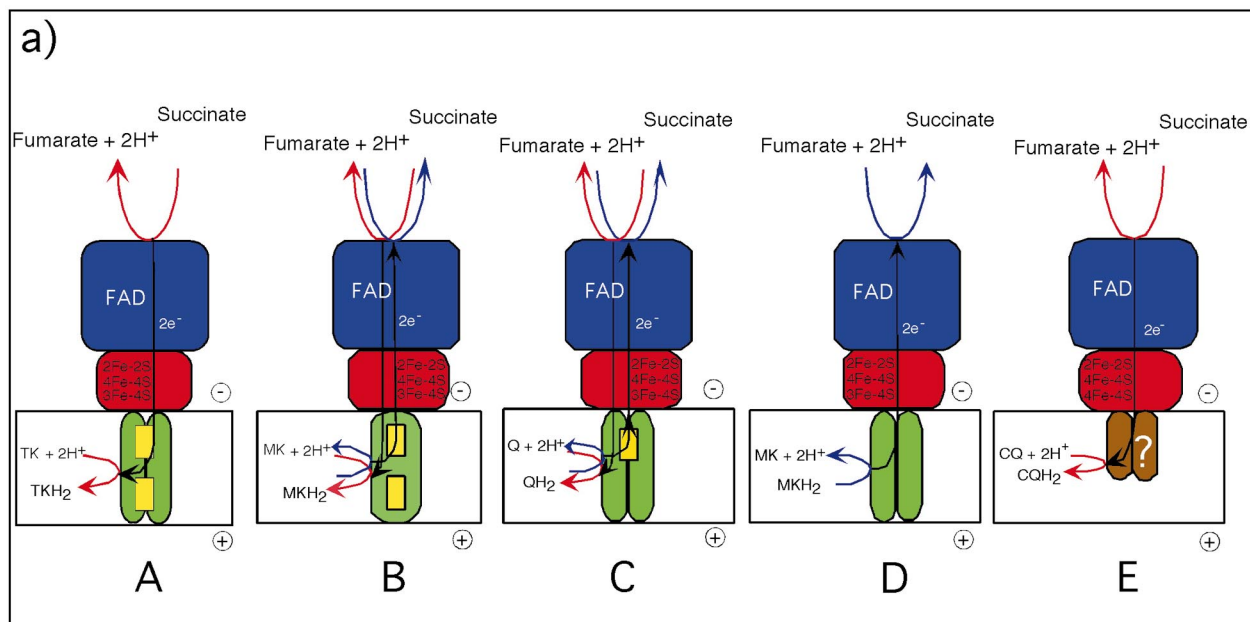
(Fig. 2c,d). The latter residue replaces the water molecule previously suggested to be the proton donor [8] based on the structure in crystal form B (Fig. 2b). The assignment as to which of the fumarate methenyl carbon atoms accepts the hydride and which the proton is currently ambiguous (Fig. 2c versus d), because data of sufficient completeness and quality for this crystal form have so far only been obtained for the complex with malonate and not yet in the presence of fumarate. Release of the product could be facilitated by movement of the capping domain away from the dicarboxylate site [8,17]. All residues implicated in substrate binding and catalysis are conserved throughout the superfamily of succinate:quinone oxidoreductases, so that this reversible mechanism is considered generally relevant for all succinate:quinone oxidoreductases.

This mechanistic interpretation of the structure is supported by the results from site-directed mutagenesis, where Arg A301 was replaced relatively conservatively by a Lys [17]. Strain FrdA-R301K contained a variant enzyme, very similar to the wild type enzyme in terms of cofactor and subunit composition, in particular a fluorescence typical for FAD covalently bound to the A subunit, but which lacked succinate dehydrogenase and fumarate reductase activity [17]. The loss in enzymatic activity is tentatively attributed to the fact that Lys ($pK_{sol} = 10.8$) cannot substitute for Arg ($pK_{sol} = 12.5$) in protonating the fumarate methenyl carbon, possibly because the protonating group is no longer close enough to protonate the fumarate methenyl group.

4. Subunit B, the iron–sulphur protein

The Cα trace of *W. succinogenes* subunit B is shown in Fig. 3a. This subunit of 27 kDa [19] consists of two domains (Fig. 1c), an N-terminal 'plant ferredoxin' domain (B1–106), binding the [2Fe–2S] iron–sulphur centre and a C-terminal 'bacterial ferredoxin' domain (B106–239) binding the [4Fe–4S] and the [3Fe–4S] iron–sulphur centres. The [2Fe–2S] iron–sulphur centre is coordinated by the Cys residues B57, B62, B65, and B77 as proposed on the basis of sequence alignments [19]. All four Cys residues are within segments that are in contact with the A subunit. The [4Fe–4S] iron–sulphur centre is ligated to the protein through Cys residues B151, B154, B157, and B218, and the [3Fe–4S] centre is coordinated by Cys residues B161, B208, and B214. The latter three residues are within segments that are in contact with the C subunit. At the position corresponding to the fourth Cys of the [4Fe–4S] centre, *W. succinogenes* QFR [3Fe–4S] centre contains a Leu. Whereas the

introduction of a Cys into *E. coli* QFR [21] could replace the native [3Fe–4S] by a [4Fe–4S] centre, this was not the case for *B. subtilis* SQR [22].

5. Subunit C, the integral membrane domain

The Cα trace of *W. succinogenes* subunit C is shown in Fig. 3b. This subunit of 30 kDa [23] contains five membrane-spanning segments with preferentially helical secondary structure. For systematic reasons within the superfamily of succinate:quinone oxidoreductases, these segments are labelled (according to [6]) I (C22–52), II (C77–100), IV (C121–149), V (C169–194), and VI (C202–237). To a varying degree, all five transmembrane segments are tilted with respect to the membrane normal, and helix IV is strongly kinked at position C137 [8]. This kink is stabilised by the side chain γ-hydroxyl of Ser C141, which, instead of its backbone NH, donates a hydrogen bond to the carbonyl oxygen of Phe C137 (Fig. 3c). As pointed out earlier [18], this feature is very similar to that found for helix F of bacteriorhodopsin (bR, PDB entry 1C3W [24]).

The planes of both haem molecules bound by the *W. succinogenes* enzyme are approximately perpendicular to the membrane surface and their interplanar angle is 95° [8]. The axial ligands to the 'proximal' haem b_P are His C93 of transmembrane segment II and His C182 of transmembrane segment V (Fig. 3d). This causes haem b_P to be located towards the cytoplasmic surface of the membrane, and thus towards the [3Fe–4S] iron–sulphur centre. Hydrogen bonds and salt bridges with the propionate groups of haem b_P are formed with the side chains of residues Gln C30, Ser C31, Trp C126 and Lys C193 [8] (Fig. 3d). Thus, side chains from the residues of the first four transmembrane segments are involved in the binding of haem b_P [8], which underscores the structural importance of the bound haem [25]. The axial ligands to the 'distal' haem b_D are His C44 of transmembrane segment I and His C143 of transmembrane segment IV ([8], figure 6b), demonstrating that all four haem axial ligands had been correctly predicted by sequence alignment [23] and site-directed mutagenesis [25]. As noted earlier [8], the binding of the two haem *b* molecules described here is very different from that described for the cytochrome bc_1 complex [26]. In *W. succinogenes* QFR, the axial ligands for haem binding are located on four different transmembrane segments. In the cytochrome bc_1 complex, only two transmembrane segments are involved, each providing two axial haem *b* ligands. One consequence

$\rightarrow$

Fig. 2. *W. succinogenes* QFR subunit A and the possible mechanism of fumarate reduction. Figures modified from [17]. a: The first three domains of subunit A and the different relative orientations of the capping domain in crystal forms B (PDB entry 1QLB [8], black Cα trace) and C (PDB entry 1E7P [17], coloured Cα trace). In the latter case, the FAD-binding domain, the capping domain, the helical domain are drawn in blue, green, and red, respectively. In the centre, the histidyl-FAD, the bound fumarate of crystal form 'B' and the location of residue Arg A301 in both structures are indicated as stick models. Carbon, nitrogen, oxygen, and phosphorus atoms are shown in yellow, blue, red, and light green, respectively. The QFR crystal form 'B' Arg A301 carbon atoms are drawn in green. For a better view of these structural differences, short animations with the structures of the the two crystal forms as starting and ending structures are available at http://www.mpibp-frankfurt.mpg.de/lancaster/febs2001/fig2a.swf and http://www.mpibp-frankfurt.mpg.de/lancaster/febs2001/fig2b.swf, respectively. b: Comparison of crystal forms 'C' (PDB entry 1E7P, carbon atoms in yellow, complex with malonate) and 'B' (PDB entry 1QLB, carbon atoms in green, complex with fumarate) at the site of fumarate reduction in subunit A. The isolated red spheres correspond to the oxygen atoms of two water molecules in PDB entry 1QLB. The dicarboxylate-binding site in the form C crystal for which a diffraction data set could be obtained contained the smaller competitive inhibitor malonate rather than fumarate, but this structural difference is negligible compared to the large structural other differences shown here. c and d: Alternate possible mechanisms of fumarate reduction in *W. succinogenes* QFR involving the residues shown in b for the crystal form C. Since the precise location of the bound fumarate molecule in this crystal form is not yet known, it could either be the β-methenyl group (c) or the α-methenyl group (d) which which is reduced by hydride transfer from the N5 position of FADH⁻. This is coupled to proton transfer to the respective other methenyl group from the side chain of Arg A301.
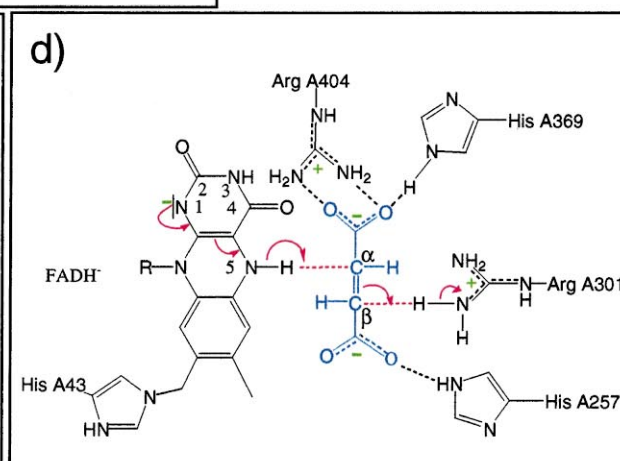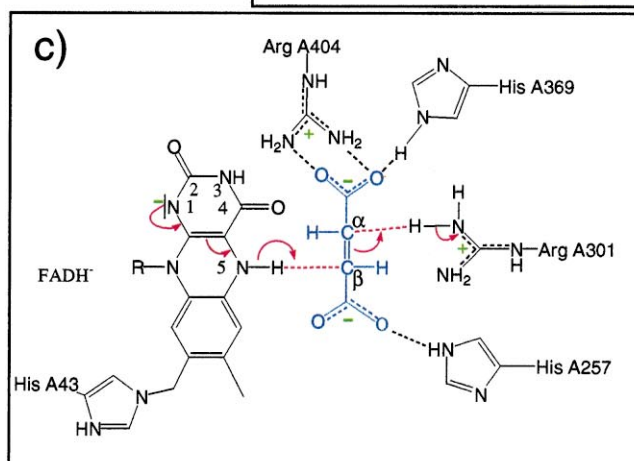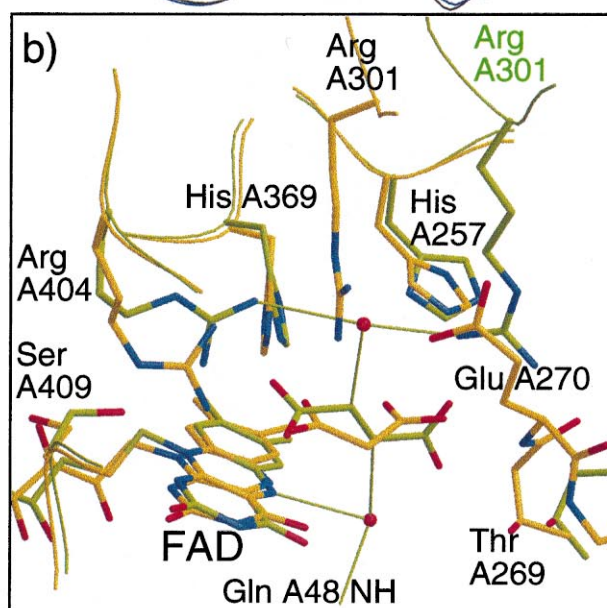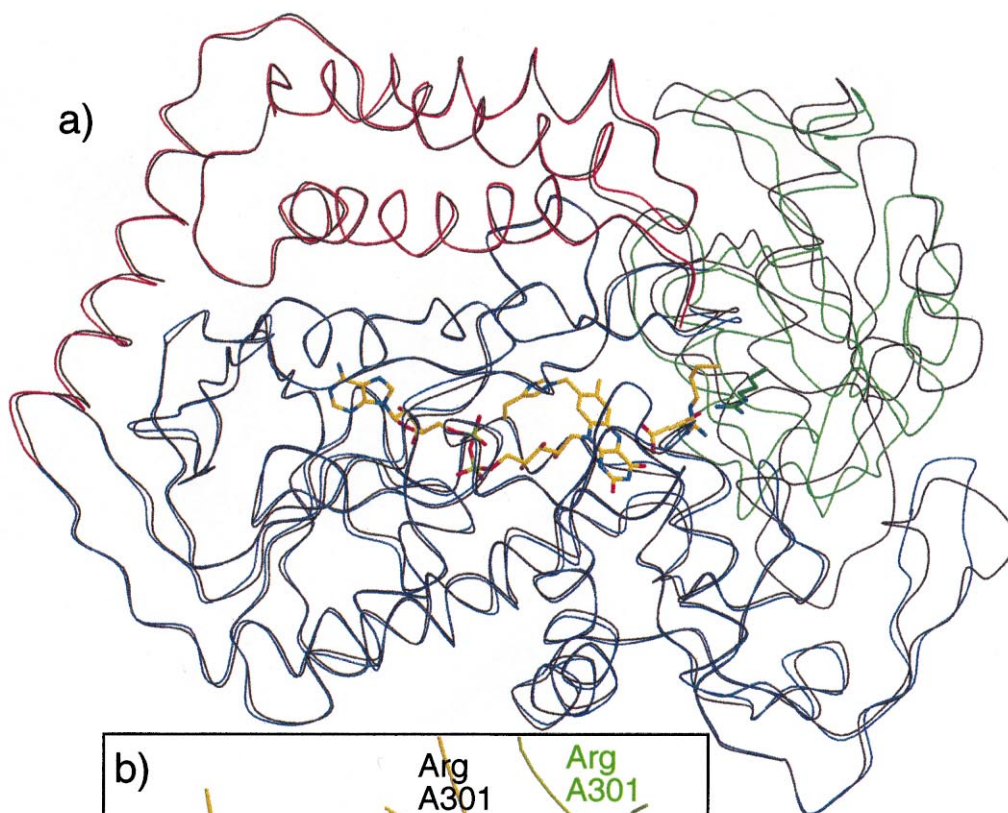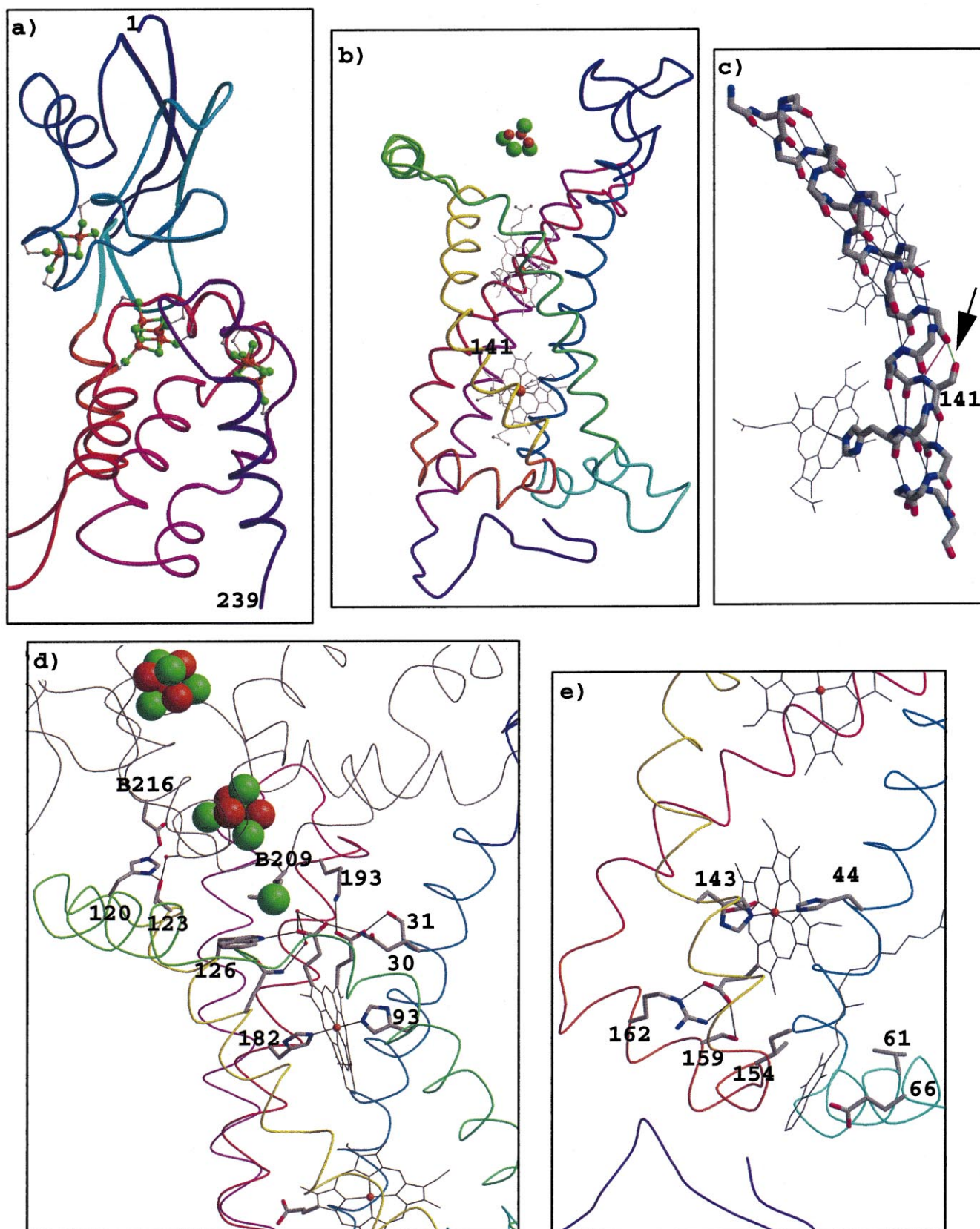
of this difference is that the distance between the two haem iron centres is distinctly shorter in QFR (15.6 Å) than it is in the cytochrome bc_1 complex (21 Å).

Residues of *W. succinogenes* QFR subunit C conserved among the succinate:quinone oxidoreductases from ε-proteo-bacteria [27] are concentrated around the haem groups and the contact surface with subunit B (Fig. 3d). However, a distal 'rim' of conserved residues is also apparent involving residues

Fig. 3. *W. succinogenes* QFR subunits B and C. a: Subunit B, the iron–sulphur protein of *W. succinogenes* QFR. The Cα trace is drawn in blue (N-terminal [2Fe–2S] domain, residues B1–106) and orange/pink/purple (C-terminal [7Fe–8S] domain, B106-B239). From top left to bottom right, the iron–sulphur clusters are [2Fe–2S], [4Fe–4S], [3Fe–4S]. The N- and C-terminus are labelled by their residue number. b: Subunit C, the dihaem cytochrome *b* of *W. succinogenes* QFR (stereo views). Also shown are the proximal (upper) and distal (lower) haem groups and the position of the [3Fe–4S] cluster (top), which is bound by the B subunit (Fig. 4). Selected C subunit residues are labelled by their residue number. The Cα trace is drawn in dark blue (N-terminus), blue (transmembrane helix I), light blue (periplasmic I–II connection), blue-green (transmembrane helix II), green (cytoplasmic II–IV connection), yellow (transmembrane helix IV), orange (periplasmic IV–V connection), red (transmembrane helix V), pink (transmembrane helix VI), and purple (C-terminus). c: Transmembrane helix IV from *W. succinogenes* QFR (PDB entry 1QLA [8]). Hydrogen bonding interactions are indicated by black dashed lines. The highlighted hydrogen bond donated from the Ser side chain is indicated in green. The corresponding interaction donated by the backbone NH for a standard α-helix is indicated in red. The distance between Ser C141 N and Phe C137 O (indicated in red) is 4.0 Å, the distance between Ser C141 Oγ and Phe C137 O (indicated in green) is 2.8 Å. d: Selected proximal residues in the structure of *W. succinogenes* QFR that are conserved in the QFR enzymes of other ε-proteobacteria. The Cα trace of subunit C is colour-coded as described for Fig. 3b. In addition, the Cα trace of subunit B is shown in black. Also indicated are two conserved B subunit residues (B209 and B216). All other labelling refers to selected proximal C subunit residues. The following prosthetic groups are included from the top left to the bottom right: the [4Fe–4S] cluster, the [3Fe–4S] cluster, the proximal haem and the distal haem. e: Selected distal C subunit residues are labelled. The proximal (upper) and distal (lower) haem are included as is the tentative menaquinol-binding position deduced in [16]. Transmembrane helices II and VI have been omitted for clarity.
←

Glu C66, Ile C154, Ser C159, and Arg C162 (Fig. 3e). While the latter two residues interact with a propionate of haem b_D, Glu C66 and Ile C154 are likely to play a role in the binding of the menaquinol substrate, as discussed below.

6. Relative orientation of soluble and membrane-embedded subunits

The structure of *E. coli* QFR can be superimposed on the structure of *W. succinogenes* QFR based on the hydrophilic subunits A and B (figures 3c and 6b in [8]). This similarity in structure was expected based on sequence comparisons. However, in this superimposition, the membrane-embedded subunits cannot be aligned. In an alternate superimposition, the transmembrane subunits C and D of the *E. coli* enzyme can be overlayed on to the *W. succinogenes* C subunit (figures 3c and 6b in [8]). Compared to the former superimposition, the latter involves a rotation around the membrane normal of approximately 180° and an orthogonal 25° rotation. This immediately leads to two important conclusions [8]. First, the structures of the transmembrane subunits carrying no haems and two haems, respectively, can be aligned to a significant degree, although only 11 of the aligned residues are identical. Second, the relative orientation of the soluble subunits and the transmembrane subunits is different in the QFR complexes from the two species.

7. The site of menaquinol oxidation/menaquinone reduction

The site of menaquinol oxidation on the dihaem cytochrome *b* subunit of *W. succinogenes* QFR is not known. No density for a quinol or quinone could be found in any of the three crystal forms of the oxidised enzyme. No specific inhibitor of menaquinol oxidation by *W. succinogenes* QFR has been identified. The *E. coli* QFR coordinate set 1FUM [15] contains models for two menaquinone molecules per ABCD monomer. Although some of the atomic temperature factors of the quinone ring atoms are larger than 100 Å², indicating that these quinone models may not be well defined, these models were included in figures 6b and c in [8] for comparison. This structural alignment showed that the *E. coli* QFR menaquinone models are at positions occupied by haem propionates in *W. succinogenes* QFR [8].

In the latter crystal structure, a cavity which extends from the hydrophobic phase of the membrane, close to the distal haem b_D, to the periplasmic aqueous phase could accommodate a menaquinol molecule, after minor structural alterations [16], which are consistent with experimentally observed structural differences for the presence and absence of a quinone substrate [28]. A glutamate residue (Glu C66) lines the cavity and could accept a hydrogen bond from one of the hydroxyl groups of menaquinol (Fig. 3e). Replacement of Glu C66 by a glutamine residue resulted in a mutant which did not catalyse quinol oxidation by fumarate, whereas the activity of fumarate reduction was not affected by the mutation [16]. X-ray crystal structure analysis of the Glu C66→Gln variant enzyme ruled out significant structural alterations. The midpoint potentials of the two haem groups of subunit C were not significantly affected. These results indicate that the inhibition of quinol oxidation activity in the mutant enzyme is due to absence of the carboxyl group of Glu C66. Thus it was concluded that Glu C66, which is conserved in the QFR enzymes from the ε-proteobacteria *C. jejuni* and *H. pylori*, is an essential constituent of the menaquinol oxidation site [16] close to haem b_D (Fig. 3e).

8. Electron and proton transfer

For the function of QFR, electrons have to be transferred from the quinol-oxidising site in the membrane to the fumarate-reducing site, protruding into the cytoplasm. The arrangement of the prosthetic groups in the QFR dimer is displayed in Fig. 4a together with the edge-to-edge distances relevant for electron transfer as defined in [29]. It has been shown for other electron transfer proteins, that physiological electron transfer occurs if such distances are shorter than 14 Å, but not if they are longer than 14 Å [29]. In the case of *W. succinogenes* QFR, this indicates that physiological electron transfer can occur between the six prosthetic groups of one QFR heterotrimeric complex, but not between the two QFR complexes in the dimer.

The fumarate molecule is in van der Waals contact with the isoalloxazine ring of FAD. The edge-to-edge distance between the headgroup of the menaquinol model shown in Fig. 4a and haem b_D is 6.7 Å. The linear arrangement of the prosthetic groups in one QFR complex therefore provides one straightforward pathway by which electrons could be transferred efficiently from the menaquinol-oxidising site via the two haem groups, the three iron–sulphur centres and the FAD to the site of fumarate reduction.

The two haem groups have different oxidation–reduction potentials [30], one is the 'high-potential' haem b_H
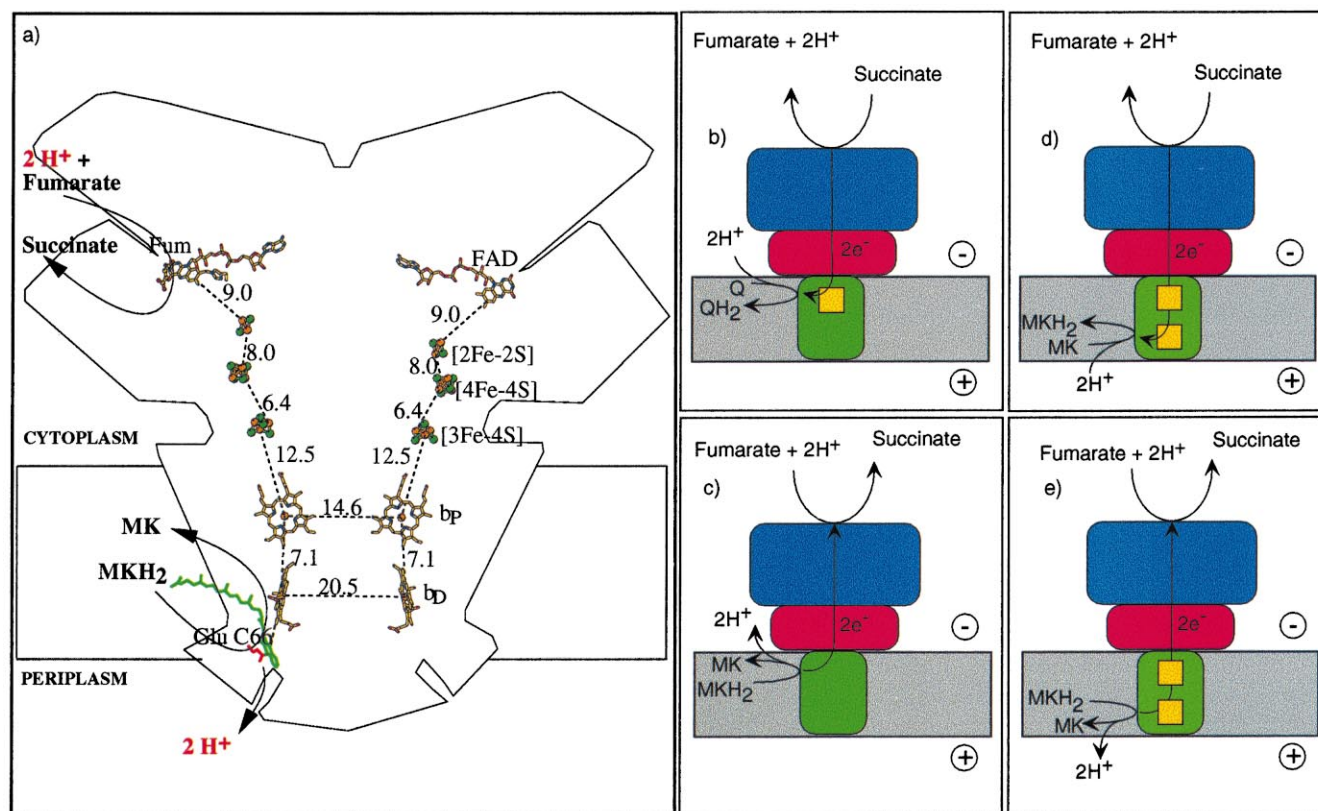
Fig. 4. The coupling of electron and proton flow in succinate:quinone oxidoreductases in anaerobic (a, c, e) and aerobic respiration (b, d), respectively. Positive and negative sides of the membrane are described for Fig. 1. a: Hypothetical transmembrane electrochemical potential as suggested by the essential role of Glu C66 for menaquinol oxidation by *W. succinogenes* QFR [16]. The prosthetic groups of the *W. succinogenes* QFR dimer are displayed (coordinate set 1QLA [8]). Distances between prosthetic groups are edge-to-edge distances in Å as defined in [29]. Drawn in red is the side chain of Glu C66. The tentative model of menaquinol binding (drawn in green) is taken from [16]. The position of bound fumarate (Fum) is taken from PDB entry 1QLB [8]. b and c: Electroneutral reactions as catalysed by C-type SQR enzymes (b) and D-type *E. coli* QFR (c). d and e: Utilisation (d) and generation (e) of a transmembrane electrochemical potential as possibly catalysed by A-type and B-type enzymes.

($E_M = -20$ mV or -15 mV for the membrane-bound [30] and detergent-solubilised [16] QFR enzyme, respectively), the other the 'low-potential' haem b_L ($E_M = -200$ mV [30] and -150 mV [16], respectively). It has not yet been established which of the haems b_P and b_D corresponds to b_L and b_H in *W. succinogenes* QFR.

Because of its very low midpoint potential ($E_m < -250$ mV [31]), the [4Fe–4S] iron–sulphur centre has been suggested not to participate in electron transfer (see [2] for a discussion). However, the determined low potential may be an artefact due to anti-cooperative electrostatic interactions between the redox centres [32]. The position of the [4Fe–4S] centre as revealed in the structures of *W. succinogenes* QFR and *E. coli* QFR is highly suggestive of its direct role in electron transfer from the [3Fe–4S] centre to the [2Fe–2S] centre. Despite this major thermodynamically unfavourable step, the calculated rate of electron transfer is on a microsecond scale, demonstrating that this barrier can easily be overcome by thermal activation as long as the electron transfer chain components are sufficiently close to promote intrinsically rapid electron tunneling [33].

In addition to the transfer of electrons, two protons are bound upon fumarate reduction (see reaction 1) and two protons are liberated upon menaquinol oxidation (see reaction 2). The protons consumed upon fumarate reduction are undoubtedly bound from the cytoplasm (see Fig. 4a). The experimen-

tal results on intact bacteria, with inverted vesicles or liposomes containing *W. succinogenes* QFR discussed by Kröger et al. [34,35] suggest that the oxidation of menaquinol by fumarate as catalysed by *W. succinogenes* QFR is an electroneutral process. The protons formed by menaquinol oxidation have therefore been assumed to be released to the cytoplasmic side of the membrane where they balance the protons consumed by fumarate reduction.

However, the essential role of Glu C66 for menaquinol oxidation demonstrated in Ref. [16] contrasts this interpretation. Most probably, this residue acts by accepting a proton formed by menaquinol oxidation. Glu C66 lines a cavity which extends to the periplasmic aqueous phase. This strongly suggests that the protons liberated during menaquinol oxidation are released on the periplasmic side of the membrane. In summary, the location of the catalytic sites of fumarate reduction and menaquinol oxidation in the structure indicates that quinol oxidation by fumarate is an electrogenic process in *W. succinogenes*, in contrast to the presently available results of experimental measurements for *W. succinogenes* QFR.

An overview of the different possibilities of electron and proton transfer in succinate:quinone oxidoreductases is shown in Fig. 4b–e. In mitochondrial complex II and other C-type enzymes, such as SQR from *P. denitrificans* and *E. coli*, electron transfer from succinate to ubiquinone does not lead to the generation of a transmembrane electrochemical

potential (see [36] for a review), since the protons released by succinate oxidation are on the same side of the membrane as those consumed by quinone reduction (Fig. 4b). It is unlikely that transmembrane electron transfer occurs in the *E. coli* QFR, because of the large edge-to-edge distance of ∼25 Å between the two quinone models [8]. Therefore, it is most likely that quinol oxidation occurs at a proximal site (Fig. 4c). Succinate oxidation by menaquinone, an endergonic reaction under standard conditions, is catalysed by a B-type succinate:quinone oxidoreductase in Gram-positive bacteria, e.g. *B. subtilis*. There is experimental evidence indicating that succinate oxidation by menaquinone in *B. subtilis* is driven by the electrochemical proton potential ([37], Fig. 4d). This is the analogous reaction to that suggested for *W. succinogenes* QFR (Fig. 4e), but in the opposite direction [18,36]. Recent experimental results indeed indicate that *B. subtilis* SQR generates a proton potential when functioning as a QFR ([38], Fig. 4e).

References

[1] Lemma, E., Hägerhäll, C., Geisler, V., Brandt, U., von Jagow, G. and Kröger, A. (1991) Biochim. Biophys. Acta 1059, 281–285.
[2] Hägerhäll, C. (1997) Biochim. Biophys. Acta 1320, 107–141.
[3] Saraste, M. (1999) Science 283, 1488–1493.
[4] Kröger, A. (1978) Biochim. Biophys. Acta 505, 129–145.
[5] Kröger, A., Geisler, V., Lemma, E., Theis, F. and Lenger, R. (1992) Arch. Microbiol. 158, 311–314.
[6] Hägerhäll, C. and Hederstedt, L. (1996) FEBS Lett. 389, 25–31.
[7] Hederstedt, L. (1999) Science 284, 1941–1942.
[8] Lancaster, C.R.D., Kröger, A., Auer, M. and Michel, H. (1999) Nature 402, 377–385.
[9] Schäfer, G., Engelhard, M. and Müller, V. (1999) Microbiol. Mol. Biol. Rev. 63, 570–620.
[10] Gomes, C.M., Lemos, R.S., Teixeira, M., Kletzin, A., Huber, H., Stetter, K.O., Schäfer, G. and Anemüller, S. (1999) Biochim. Biophys. Acta 1411, 134–141.
[11] Singer, T.P. and McIntire, W.S. (1984) Methods Enzymol. 106, 369–378.
[12] Walker, W.H. and Singer, T.P. (1970) J. Biol. Chem. 245, 4224–4225.
[13] Kenny, W.C. and Kröger, A. (1977) FEBS Lett. 73, 239–243.
[14] Weiner, J.H. and Dickie, P. (1979) J. Biol. Chem. 254, 8590–8593.
[15] Iverson, T.M., Luna-Chavez, C., Cecchini, G. and Rees, D.C. (1999) Science 284, 1961–1966.
[16] Lancaster, C.R.D., Groß, R., Haas, A., Ritter, M., Mäntele, W.,
Simon, J. and Kröger, A. (2000) Proc. Natl. Acad. Sci. USA 97, 13051–13056.
[17] Lancaster, C.R.D., Groß, R. and Simon, J. (2001) Eur. J. Biochem. 268, 1820–1827.
[18] Lancaster, C.R.D. and Kröger, A. (2000) Biochim. Biophys. Acta 1459, 422–431.
[19] Lauterbach, F., Körtner, C., Albracht, S.P., Unden, G. and Kroeger, A. (1990) Arch. Microbiol. 154, 386–393.
[20] Lancaster, C.R.D., in: Membrane Protein Purification and Crystallization: A Practical Guide, Second Edition (Hunte, C., Schägger, H. and von Jagow, G., Eds.), Academic Press, San Diego, CA, in press.
[21] Mandori, A., Cecchini, G., Schröder, I., Gunsalus, R.P., Werth, M.T. and Johnson, M.K. (1992) Biochemistry 31, 2703–2712.
[22] Hägerhäll, C., Sled, V., Hederstedt, L. and Ohnishi, T. (1995) Biochim. Biophys. Acta 1229, 356–362.
[23] Körtner, C., Lauterbach, F., Tripier, D., Unden, G. and Kroeger, A. (1990) Mol. Microbiol. 4, 855–860.
[24] Luecke, H., Schobert, B., Richter, H.T., Cartailler, J.-P. and Lanyi, J.K. (1999) J. Mol. Biol. 291, 899–911.
[25] Simon, J., Groß, R., Ringel, M., Schmidt, E. and Kröger, A. (1998) Eur. J. Biochem. 251, 418–426.
[26] Xia, D., Yu, C.A., Kim, H., Xian, J.Z., Kachurin, A.M., Zhang, L., Yu, L. and Deisenhofer, J. (1997) Science 277, 60–66.
[27] Lancaster, C.R.D. and Simon, J., Biochim. Biophys. Acta, in press.
[28] Lancaster, C.R.D. and Michel, H. (1997) Structure 5, 1339–1359.
[29] Page, C.C., Moser, C.C., Chen, X. and Dutton, P.L. (1999) Nature 402, 47–52.
[30] Kröger, A. and Innerhofer, A. (1976) Eur. J. Biochem. 69, 497–506.
[31] Unden, G., Albracht, S.P.J. and Kröger, A. (1984) Biochim. Biophys. Acta 767, 460–469.
[32] Salerno, J.C. (1991) Biochem. Soc. Trans. 19, 599–605.
[33] Dutton, P.L., Chen, X., Page, C.C., Huang, S., Ohnishi, T. and Moser, C.C. (1998) in: Biological Electron Transfer Chains: Genetics, Composition and Mode of Operation (Canters, G.W., Vijgenboom E., Eds.), pp. 3–8, Kluwer Academic Publishers, Dordrecht.
[34] Geisler, V., Ullmann, R. and Kröger, A. (1994) Biochim. Biophys. Acta 1184, 219–226.
[35] Kröger, A., Biel, S., Simon, J., Groß, R., Unden, G. and Lancaster, C.R.D., Biochim. Biophys. Acta, in press.
[36] Ohnishi, T., Moser, C.C., Page, C.C., Dutton, P.L. and Yano, T. (2000) Structure 8, R23–R32.
[37] Schirawski, J. and Unden, G. (1998) Eur. J. Biochem. 257, 210–215.
[38] Schnorpfeil, M., Janausch, I.G., Biel, S., Kröger, A. and Unden, G. (2001) Eur. J. Biochem. 268, 3069–3074.
[39] Lancaster, C.R.D. (2001) in: Handbook of Metalloproteins, Vol. 1, (Messerschmidt, A., Huber, R., Poulos, T., and Wieghardt, K., Eds.), John Wiley and Sons, Chichester, pp. 379–401.
[40] Kraulis, P.J. (1991) J. Appl. Crystallogr. 24, 946–950.
[41] Esnouf, R.M. (1997) J. Mol. Graphics Model. 15, 132–134.
[42] Merrit, E.A. and Bacon, D.J. (1997) Methods Enzymol. 277, 505–524.